Sound & Vibration 2025, 59(3), 3143.
https://doi.org/10.59400/sv3143

Article

Physics-informed GRU model for vehicle road noise prediction: Integrating transfer path analysis and hybrid data

Yan Ma[1], Ruxue Dai[2], Tao Liu[1], Mingzheng Wang[1], Qichen Ying[2], Haibo Huang[2,*]

[1] Global R&D Center, China FAW Corporation Limited, Changchun 130013, China
[2] School of Mechanical Engineering, Southwest Jiaotong University, Chengdu 610031, China
*** Corresponding author:** Haibo Huang, huanghaibo214@foxmail.cn

CITATION

Ma Y, Dai R, Liu T, et al. Physics-informed GRU model for vehicle road noise prediction: Integrating transfer path analysis and hybrid data. Sound & Vibration. 2025; 59(3): 3143. https://doi.org/10.59400/sv3143

ARTICLE INFO

Received: 21 April 2025
Accepted: 13 June 2025
Available online: 4 July 2025

Abstract: With the continuous release of automobile market potential and the steady growth of automobile ownership, consumers' concern for automobile NVH problems makes the road noise performance directly affect the sales of automobiles. Therefore, it is of great significance to study the problem of vehicle road noise. In the actual research process, it often faces the challenge of insufficient effective sample size. In this paper, 102 sets of sample data are collected by combining the real vehicle test method and the CAE simulation method. By comparing the road noise prediction model based on the GRU algorithm with the LSTM model and the CNN model, the results show that the GRU model performs roughly similarly to the LSTM model in terms of prediction accuracy (RMSE = 2.18) and robustness (MSE = 7.66%), and the GRU model and the LSTM model are significantly better than the CNN model, but the prediction efficiency of the GRU model is significantly better than the LSTM model. Therefore, the vehicle road noise prediction model based on the GRU algorithm is optimal. This paper provides an efficient method for road noise performance analysis and prediction, which can be applied to the vehicle design and performance improvement process and provide technical support for improving vehicle comfort and market competitiveness.

Keywords: road noise; vehicle NVH; mechanism-data fusion; GRU; hybrid data

1. Introduction

The phenomenon of NVH (noise, vibration and harshness) in the process of vehicle driving is unavoidable. Obvious NVH problems will not only damage the stability, reliability, and life of the vehicle driving state but also affect the feelings of the driver and passenger [1]. Powertrain noise, wind noise, and road noise are the three major noises of automobiles. With the vigorous development of energy conservation and emission reduction and energy security in China, the electrification of automobiles has made the medium- and low-frequency structural noise caused by road roughness excitation become the main factor of automobile road noise [2,3].

Scholars at home and abroad have done a lot of research on vehicle road noise. Based on the formation mechanism of road noise, it is a common method to analyze road noise through experiments and simulations. Diez-Ibarbia et al. [4,5] carried out hammering experiments based on the TPA (transfer path analysis) method, analyzed the transfer path from the vehicle vibration source to the receiving place, and evaluated and determined the contribution of noise and vibration to the critical path. In order to overcome the shortcomings of traditional TPA, such as time-consuming and incorrect boundary conditions, Zhu et al. [6] proposed an improved TPA method using artificial excitation. With this method, noise and vibration problems can be analyzed without dismantling the mechanical system. Li et al. [7] and Vaitkus et al. [8] used a simpler

OTPA (Operational transfer path analysis) method to establish a 'reference point-target point' model based on the OTPA method to study noise control technology. On the basis of the transfer path method, a large number of experiments are needed to study the road noise problem by means of experimental methods, which are time-consuming, high cost, and difficult to guarantee the accuracy [9]. These shortcomings make CAE (computer aided engineering) technology applicable in road noise research. Rapino et al. [10] and Bartolozzi et al. [11] analyzed the vehicle road noise problem by establishing a vehicle road noise simulation model and adding tire and road factors. Su et al. [12] established the CAE model of the whole vehicle for correlation analysis, formulated a reasonable chassis optimization scheme, and improved the road noise performance of the whole vehicle. On the basis of OTPA test analysis, Yoshida et al. [13] used CAE analysis to adopt a strengthening policy for high-contribution vibration mode, thus reducing the interior noise level. Although the CAE modeling method can effectively reduce the dependence of road noise analysis on the test, it has the problems of difficult modeling, difficult parameter acquisition, and low accuracy. In summary, the traditional test method and simulation analysis method based on the mechanism have certain limitations on the study of vehicle road noise problems.

With the continuous research of many scholars in recent years, such as data-driven methods [14–17], its advantages of no deep mechanism, strong adaptability, high utilization rate of accumulated data, and high model prediction accuracy have been found, making it widely used in various fields. An and Jung et al. [18] predicted the pressure coefficient of buildings under complex non-uniform terrain based on PANN (artificial neural network based on empirical parameters) and MANN (artificial neural network based on morphology). Chen et al. [19] trained seven data-driven prediction models for the shear capacity of concrete joints, and the author studied the shear capacity of joints through the prediction models. The advantages of the data-driven method make it an effective method for studying NVH problems. At present, data-driven has shown significant advantages in studying noise and vibration problems, making it an effective tool for analyzing road noise problems. Oh et al. [20] proposed a method based on deep learning to continuously update the secondary path estimation in real time and finally realize the active control of road noise. Luo et al. [21] proposed a new method to evaluate the dominant noise sources of railways in all bogie areas by using a microphone array and a GNN (physical information neural network) model. Based on the MKL-SVR method, Sun et al. [22] efficiently predicted the sound insulation performance of the automobile system, which laid the foundation for the development of automobile-related noise reduction work and optimization design. The data-driven method can make a high degree of use of historical accumulated data [23], but it also has the disadvantages of strong dependence on the quality of the data set and poor model interpretation.

The analysis method of mechanism analysis and data-driven fusion aims to make full use of domain knowledge to guide modeling, ensure the interpretable application of the model, and ensure the efficiency and accuracy of the research problem. Due to the inefficiency of the finite element method and the lack of interpretability of the traditional data-driven method, the analysis method of mechanism analysis and data-driven fusion is being studied and applied by various industries. Guo et al. [24] introduced the differential equation of double time-varying diffusion solution in the

traditional data-driven method to analyze the chloride ion erosion problem of concrete. Cong et al. established the PINN (physical information neural network) model based on the principle of fatigue crack growth rate and verified the accuracy of the model prediction through experiments [25]. Liu et al. coupled a sorting operation into PINN [26] and proved the accuracy of PINN in predicting the potential energy curve by comparison, which provided a portable and effective method for the engineering field of origami structures. Fan et al. [27] and Jeong et al. [28] predicted the ultra-high cycle fatigue life of the structure and analyzed the structural topology optimization by combining data-driven and physical principles. Pang et al. [29] introduced a mechanism model into the data-driven model to establish a mechanism and data-driven model and used this model to study the interior noise caused by uneven roads. The mechanism and data fusion modeling method has advantages in reducing model uncertainty and data demand, and the method shows high reliability and high accuracy.

In summary, this paper uses the combination of TPA analysis and data-driven methods to predict the interior noise problem caused by road roughness mechanisms. It is summarized as a research method of self-consistent fusion of mechanism and data. This method can not only alleviate the high cost of a large number of test personnel and repeated test operations but also ensure the accuracy of road noise model prediction. The model has strong interpretability and can guide the further improvement of the model according to the prediction results.

The main contributions of this paper are as follows: 1) The empirical formula is introduced as the loss term, and the road noise problem is fused and analyzed by combining TPA analysis and data-driven methods. A road noise performance prediction model based on self-consistent fusion of mechanism and data is established. 2) A hierarchical structure of vehicle road noise with self-consistent fusion of mechanism and data is built. On the basis of avoiding the complex mechanism of the suspension system and frame system, the excitation, transmission path, and response of the vehicle body to right ear noise are emphasized. 3) The basic data are collected by the test method and the simulation method, and the sample data set of the fusion of the test data and the simulation data is generated.

The structure of the article: 1) Section 2 introduces the generation mechanism, mechanism, data self-consistent fusion theory, and GRU theory of road noise. On the basis of expounding the mechanism and data self-consistent fusion theory, the road noise hierarchical structure is built in combination with the generation mechanism of road noise. 2) Section 3 collects basic sample data through experimental methods and simulation methods. 3) According to the road noise hierarchical structure, the TPA prediction model and the GRU prediction model are built respectively, and the TPA and data-driven fusion model are used to predict the road noise problem and verify the results. 4) Section 5 summarizes the content of the paper based on the research.

2. Research methods

2.1. Road noise generation mechanism

Road noise is a medium- and low-frequency noise caused by road roughness excitation during driving. According to the different transmission routes, road noise is divided into structural sound and air sound. As shown in **Figure 1**, the road noise

structure noise is mainly caused by the vibration caused by the road excitation and the vibration caused by the resonance of the tire cavity [30–32]. The vibration is transmitted to the passenger compartment through the suspension system and the body structure and finally causes noise. Structural sound is mainly affected by the stealth of the road surface, suspension structure, body structure, tire diameter, and flat ratio. The air noise in the road noise is mainly composed of the following aspects: the first is the friction noise generated by the friction between the tire surface and the ground and the air, the second is the aerodynamic noise caused by the disturbed air flow during the rolling process of the tire, and the last is the noise generated by the continuous contact between the tire surface pattern and the groove depth and the ground. These noises are transmitted through the air and directly enter the passenger compartment and affect the ride comfort. The intensity and characteristics of the air sound are mainly determined by factors such as the surface pattern of the tire, the depth of the groove, the material of the tire, and the way the tire contacts the ground [33,34]. The vibration caused by the road excitation and the interaction between the tire and the ground tends to be transmitted and amplified through the structure, and the structural sound has a more significant impact on the overall noise level and the noise in the cockpit. At the same time, compared with air sound, structural sound can usually be more effectively controlled by optimizing the structural design of the vehicle. Therefore, this paper mainly studies the low-frequency (20 Hz–300 Hz) road noise structure sound.

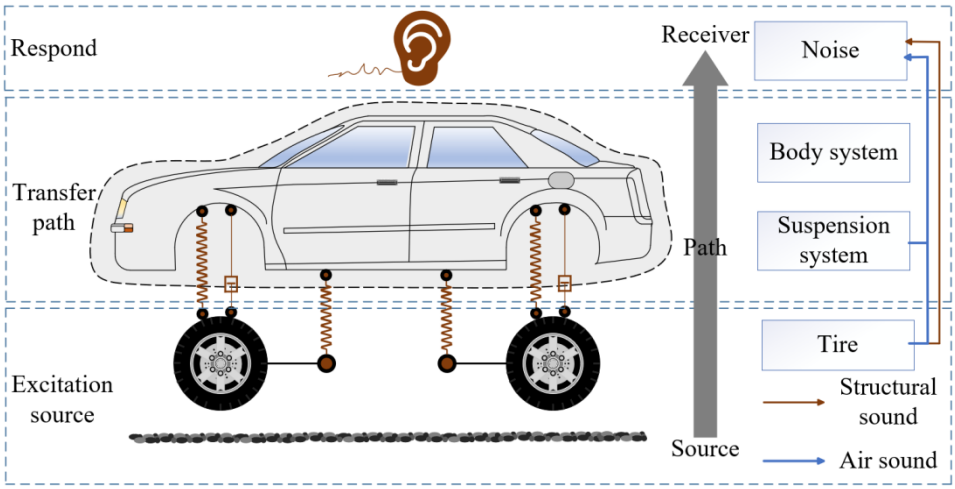

Figure 1. Vehicle road noise transfer process diagram.

2.2. Mechanism and data self-consistent fusion

This paper takes a certain type of automobile equipped with ‘front double-fork-arm and rear five-link’ suspension of FAW as the research object. The front double fork arm suspension is a commonly used suspension system for high-performance vehicles. The double fork arm suspension has many bushings and a good damping effect. At the same time, it can only change the arrangement angle of the upper and lower swing arms to design a suitable roll center, which can affect the key performance of the suspension as little as possible [35,36]. The front double fork arm suspension is composed of a front shock absorber, a front upper fork arm, and a front lower fork arm. The fork arm is shaped like a triangle (front installation point and rear installation

point). The upper fork arm of the front suspension and the shock absorber are connected to the body, and the lower fork arm is connected to the subframe.

The rear five-link is a complex multi-link suspension system, which consists of five connecting points and multiple connecting rods. It can better achieve longitudinal and lateral control, provide more precise wheel control and vehicle handling, and is usually used for high-end vehicles with high requirements for stability and comfort [37,38]. The rear five-bar linkage consists of a rear transverse tie rod, a rear transverse control arm, a rear shock absorber, a rear lower swing arm, and a rear longitudinal arm. The rear transverse tie rod and the rear transverse control arm are connected to the subframe, and the rear shock absorber, the rear lower swing arm, and the rear longitudinal arm are connected to the body.

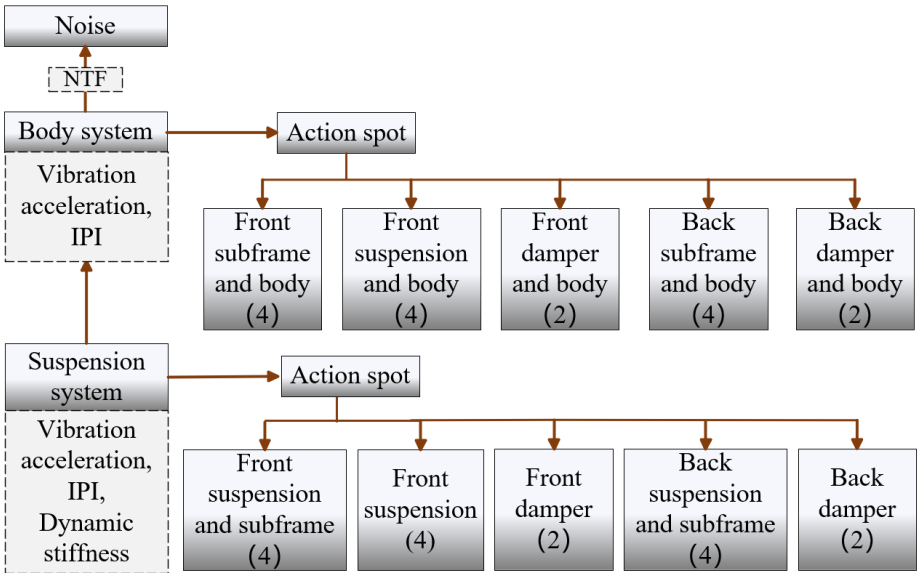

Figure 2. The main influence factors of road noise.

According to the vehicle road noise transfer process diagram shown in **Figure 1**, the influencing factors of road noise are analyzed. It can be concluded that the structure and model of the tire, suspension, and body play a key role in the effective control of road noise. Combined with the suspension structure of 'front double fork arm, rear five connecting rods', the main influencing factor diagram of road noise shown in **Figure 2** is drawn. In this diagram, we take the wheel center force of tires with different widths and thicknesses under the excitation of road roughness as the input. Since only the bushing dynamic stiffness or IPI (acceleration admittance) of the subframe is generally changed when studying new models in engineering, the IPI expression is shown in the following Equation (1). Therefore, the suspension and frame parts are simplified as a black box as a suspension system. Without studying the internal details, only the vibration acceleration, acceleration admittance, and bushing dynamic stiffness at the connection point are studied. The body part studies the vibration acceleration and the NTF (noise transfer function) from the body to the driver's right ear. The expression of NTF is shown in Equation (2). The excitation point of the front subframe includes two points connected to the front and rear installation points of the front lower swing arm. The excitation point of the rear

subframe includes two points connected to the rear lateral control arm and the rear lateral tie rod, respectively, and the output is less than 300 Hz interior noise.

$$\mathrm{IPI} = \frac{A(\omega)}{F(\omega)} \tag{1}$$

$$\mathrm{NTF} = \frac{P(\omega)}{X(\omega)} \tag{2}$$

where $A(\omega)$ represents the spectrum of the acceleration response, $F(\omega)$ represents the spectrum of the excitation force, $P(\omega)$ represents the sound pressure spectrum measured by the microphone, and $X(\omega)$ represents the acceleration or force input spectrum of the excitation point.

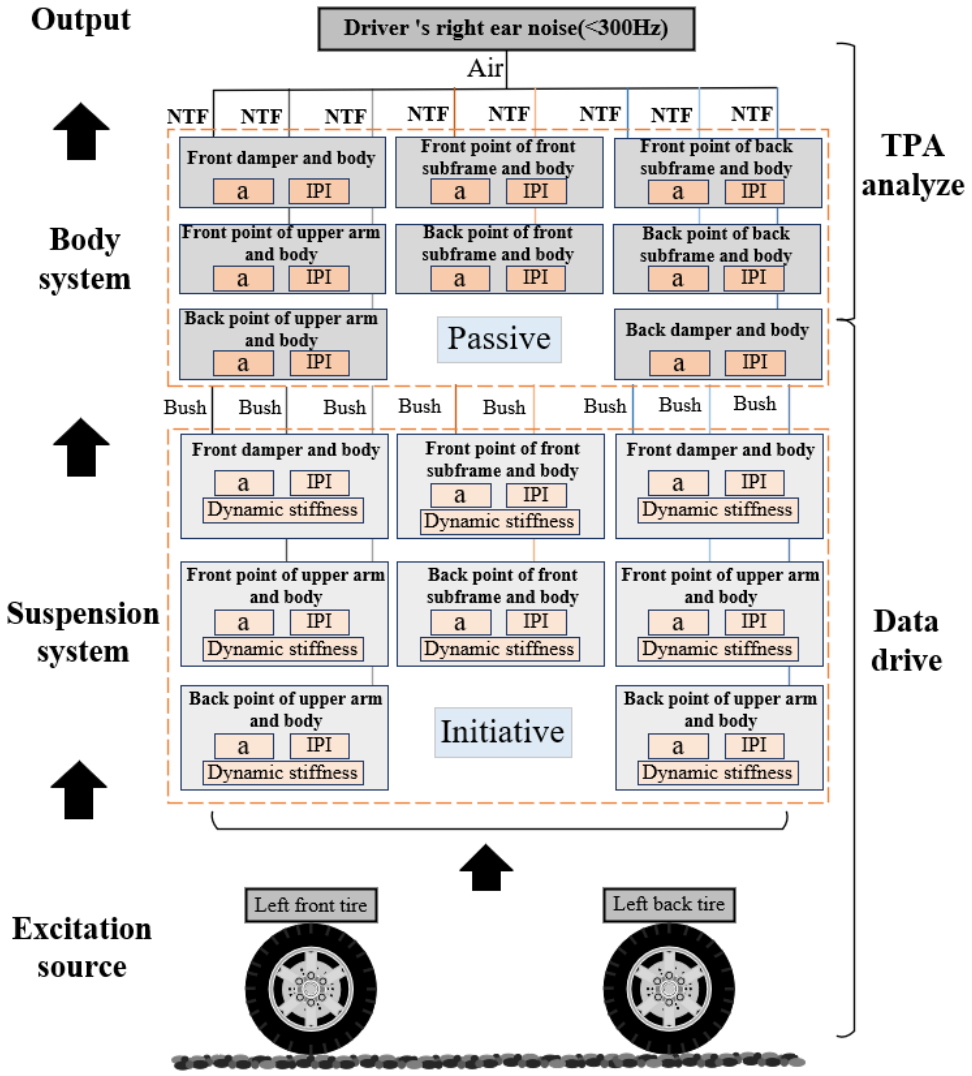

Figure 3. Road noise hierarchical architecture based on mechanism and data self-consistent fusion. a is the vibration acceleration.

Based on the above analysis, a road noise hierarchical structure with self-consistent fusion of mechanism and data, as shown in **Figure 3**, is further built. The hierarchical structure takes the left side as an example. When studying the mechanism and data self-consistent fusion model, the data-driven method is used to predict the

path of the 'excitation-suspension system-body system', which involves complex structures, while the 'body system-driver right ear noise' is predicted by the TPA method. The data-driven part can make full use of test data, simulation data, and historical data for prediction, which can improve the prediction accuracy of the complex system. The TPA method can focus on the sound source, transmission path, and response in the studied path so as to accurately predict the noise level in the vehicle. In summary, the fusion of the data-driven method and the TPA method can reduce the research cost and improve the prediction accuracy.

In addition, the empirical formula is introduced as the constraint of the prediction model, and the loss function involved is optimized and expanded to make it more in line with the requirements of low-frequency road noise prediction, forming a model prediction method of mechanism (empirical formula) and data fusion. There are three loss functions involved in this study, including the data-driven model loss function that measures the difference between the predicted value and the real value, the peak error loss function of the sequence, and the correlation loss function. The calculation formula of the model loss function is shown in Equation (3).

$$\mathrm{MSE}_d = \frac{1}{N_d}\sum_{i=1}^{N_d}\left[u_{\mathrm{pred}}(t_i^d, x_i^d; \theta,) - u_{\mathrm{real}}(t_i^d, x_i^d)\right]^2 \tag{3}$$

where N_d denotes the number of data points, $u_{\mathrm{pred}}(t_i^d, x_i^d; \theta,)$ represents the predicted value of the model, $u_{\mathrm{real}}(t_i^d, x_i^d)$ represents the real value (label value), The smaller the loss value is, the closer the predicted value of the model is to the real value.

The loss function calculation the Equation of the peak error is as follows:

$$\mathrm{MSE}_p = \frac{1}{N_p}\sum_{i=1}^{N_p}\left[u_{\mathrm{pred}}(0, x_p^{\mathrm{peak}}; \theta,) - u_{\mathrm{real}}(0, x_p^{\mathrm{peak}})\right]^2 \tag{4}$$

where N_p is the number of data points near the peak of the sequence, $u_{\mathrm{pred}}(0, x_p^{\mathrm{peak}}; \theta,)$ represents the predicted value of the neural network for the *p*-th initial data point x_p^{peak} under the parameter θ, and $u_{\mathrm{real}}(0, x_p^{\mathrm{peak}})$ represents the real value (label value) of the *p*-th initial data point x_p^{peak} under the parameter θ. The loss term calculates the mean square error between the neural network output and the real value near the characteristic peak position to ensure that the neural network output matches the real value of the characteristic peak.

The calculation method of the correlation loss function is shown in Equation (5). The correlation is measured by Pearson's correlation coefficient, which is fast and efficient. It is defined as 1 minus the Pearson correlation coefficient obtained. When the predicted value is completely correlated with the true value, the loss is 0; when the predicted value is completely unrelated to the true value, the loss is 1, thus effectively regulating the process of network training.

$$\mathrm{MSE}_r = 1 - \frac{\frac{1}{N_r}\sum_{i=1}^{N_r}\left[(u_{\mathrm{pred}}^r - \bar{u}_{\mathrm{pred}})(u_{\mathrm{real}}^r - \bar{u}_{\mathrm{real}})\right]}{\sqrt{\sum_{i=1}^{N_r}\left[(u_{\mathrm{pred}}^r - \bar{u}_{\mathrm{pred}})^2\right]\sum_{i=1}^{N_r}\left[(u_{\mathrm{real}}^r - \bar{u}_{\mathrm{real}})^2\right]}} \tag{5}$$

where N_r represents the number of data points, $\bar{u}_{\text{pred}}$ is the average value of the model prediction results, and $\bar{u}_{\text{real}}$ is the average value of the true value. The correlation loss function measures the correlation between the predicted value and the real value and characterizes the linear relationship between the predicted value and the real value.

Based on the above analysis, this paper builds a hierarchical structure that integrates mechanism features such as IPI and NTF and data features such as vibration acceleration and structural stiffness parameters. A prediction model including TPA analysis and data-driven joint modeling is established, and empirical physical constraints are introduced into the prediction process through three loss functions. Finally, a road noise modeling method with self-consistent fusion of mechanism and data is formed. This method not only improves the prediction performance but also effectively enhances the interpretability of the model by introducing intermediate parameters with physical meaning and empirical loss terms closely related to the prediction target.

2.3. Brief description of GRU theory

GRU (Gated Recurrent Unit) is a kind of RNN (recurrent neural network), which is similar to LSTM (Long-Short Term Memory). It is also proposed to solve the problems of the complex structure of long short-term memory networks and gradients in backpropagation [39–42]. GRU combines the input gate and forgetting gate of LSTM, which is called the update gate. The network structure of the three gates is simplified to a network structure with only an update gate and a reset gate, and the hidden state calculation method of the recurrent neural network is modified, as shown in **Figure 4**.

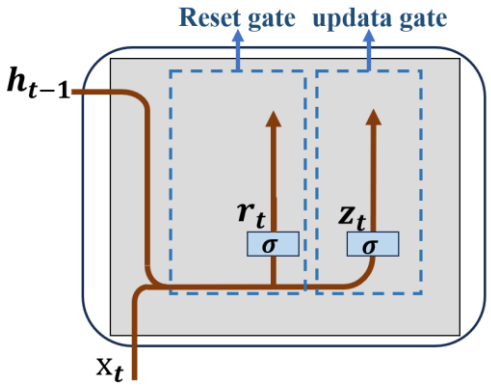

Figure 4. Reset gate and update gate in GRU.

where r_t represents the reset gate, and z_t represents the update gate. The reset gate is responsible for controlling the number and degree of forgotten information. The update gate determines whether the memory information at the previous moment can continue to be transmitted to the current moment or determines the retention ratio of the information at the previous moment at the current moment and the degree to which the information at the current moment is transmitted backward. GRU abandons the traditional linear self-updating memory unit but directly implements the linear self-updating process inside the hidden state unit by applying the gating mechanism. For a

given time step *t*, assume that the input is a small batch of $X_t \in R^{nd}$, where *n* represents the number of samples, *d* represents the number of inputs, and the hidden state of the previous time step is $h_{t-1} \in R^{nh}$, where *h* represents the number of hidden units. The calculation of the reset gate $r_t \in R^{nh}$ is shown in Equation (6), where σ represents the sigmoid activation function:

$$r_t = X_t W_{xr} + h_{t-1} W_{hr} + b_r \tag{6}$$

The calculation of the update gate $z_t \in R^{nh}$ is shown in Equation (7):

$$z_t = X_t W_{xz} + h_{t-1} W_{hz} + b_z \tag{7}$$

where W_{xr}, W_{xz}, W_{hr}, and W_{hz} are all weight parameters; $b_r \in R^h$ and $b_z \in R^h$ are bias parameters; and the sigmoid function is used to convert the input value to between 0 and 1. When the r_t term of the reset gate is close to 1, the network will be close to the ordinary recurrent neural network. For all items close to 0 in the reset gate r_t, the candidate hidden state is the result of a multi-layer perceptron with X_t as input. Where tanh represents the activation function.

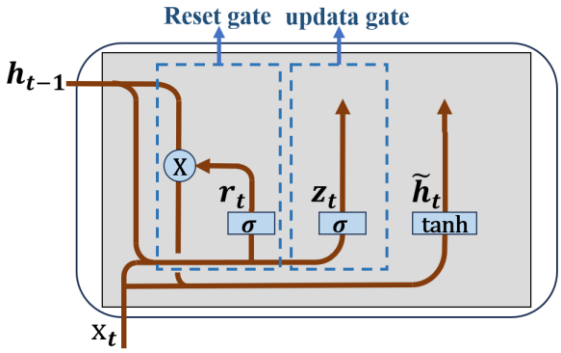

Figure 5. Calculating candidate hidden states in GRU.

Therefore, any pre-existing hidden state will be reset to the default value. The calculation process of the reset gate is shown in **Figure 5**, and the calculation result is only a candidate hidden state, which still needs to be combined with the calculation of the update gate z_t to obtain the final effect. The newly generated hidden state $h_t \in R^{nh}$ depends on the old state h_t and the new candidate state $\tilde{h}_t$. The final calculation method of GRU is shown in Equation (8):

$$\text{GRU} = h_t z_t * h_{t-1} + (1 - z_t) * \tilde{h}_t \tag{8}$$

When the update gate is close to 1, the model will maintain the original state unchanged. At this time, the processing of relevant information can be regarded as neglect, ignoring the information coming from X_t, thus effectively skipping the dependent *t* term. Therefore, when the update gate is close to 1, this step is actually simplified. Conversely, if the update gate is close to 0, the new hidden state is closely related to the candidate hidden state. The GRU method not only effectively alleviates the problem of gradient disappearance and gradient explosion in the recurrent network but also can more accurately capture the deep relationship between the time steps across the larger sequences. **Figure 6** is the GRU calculation flow after the update gate works.

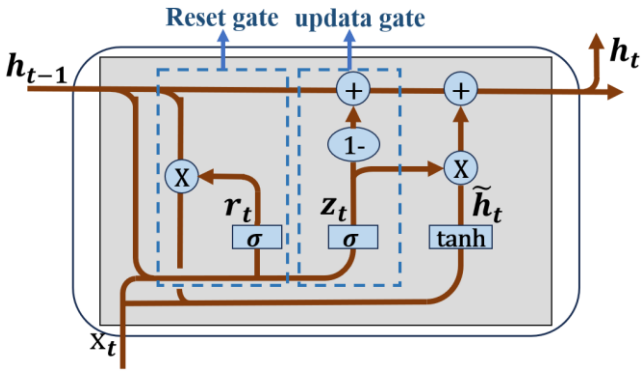

Figure 6. Computational hidden state in GRU.

3. Data collection and processing

3.1. Test data collection

The test sample vehicle of this paper is a certain type of automobile of China FAW Group. Based on the hierarchical structure built in Section 2.2, the road real vehicle test is carried out to collect the vibration data, the origin dynamic stiffness (IPI), and the bushing dynamic stiffness of the active end of the connection point between the chassis system and the body system; the vibration data and the origin dynamic stiffness (IPI) of the passive end of the connection point between the chassis system and the body system; and the noise data of the driver's right ear in the vehicle. Based on GB/T 18697-2002 vehicle interior noise measurement method [43], this paper uses LMS SCADAS Mobile data acquisition software and hardware system, a sound pressure sensor, and a three-way vibration acceleration sensor from LMS Company in Belgium to carry out a vehicle road noise road test.

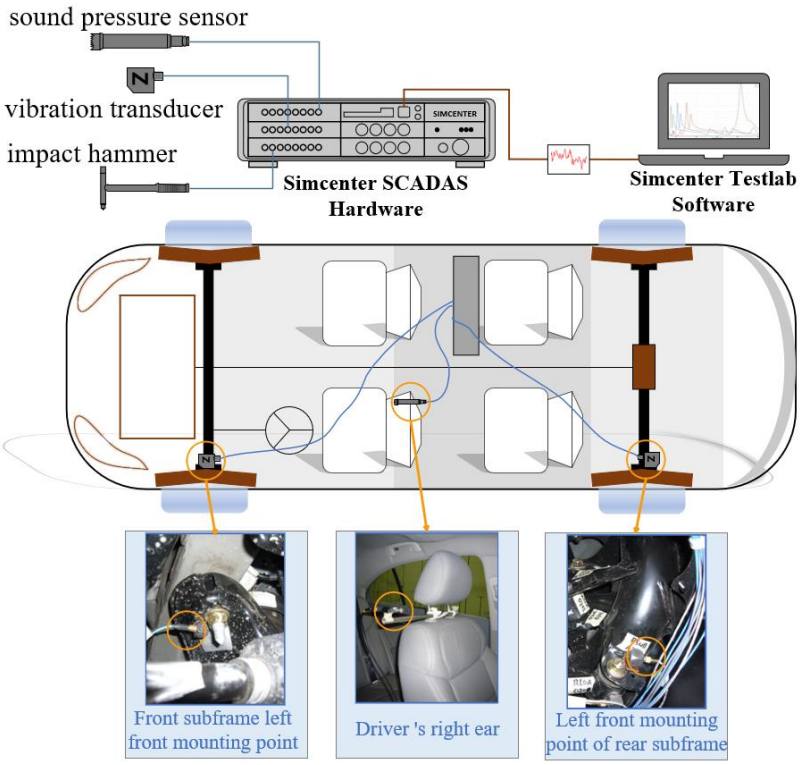

Figure 7. Sensor layout diagram.

Due to the limitation of hardware equipment, the test assumes that the vibration of the left and right sides of the vehicle is the same, so the unilateral vibration data is collected. The vertical coordinate is (0.7 ± 0.05) m above the intersection line of the seat surface and the backrest surface, and the horizontal coordinate is (0.20 ± 0.02) m from the center of the seat to the right. The sound pressure sensor is arranged to collect noise data. The 32 excitation points determined by the analysis of the main influencing factors of road noise need to be arranged with three-way acceleration sensors. The layout of each sensor on one side is shown in **Figure 7**.

When collecting transfer function data such as IPI and NTF, a hammer is used to strike the loading point short and fast. The sound pressure sensor, three-way acceleration sensor, and hammer are connected to the data acquisition instrument through a one-way line or a three-way line. The data acquisition instrument collects the noise and vibration data and submits it to the data analysis software for analysis. Under the condition of sunny weather, no three-dimensional buildings or other large objects that can reflect noise near both sides of the road, and the road environment is asphalt pavement. The vibration signal sampling frequency is set to 25,600 Hz, the noise sampling frequency is set to 51,200 Hz, and the sampling time is set to 60 s. To ensure that in addition to the necessary testers and drivers, the vehicle has no other excess load under the premise of the test site to 60 km/h, this typical urban road speed forward. Through the above test method, the real vehicle road test was carried out, and 2 sets of vehicle sample data were collected.

Taking noise data as an example, the noise sampling frequency is set to 51,200 Hz. The main purpose is to ensure that the collected noise data can cover the human ear's audible range of 20–20,000 Hz. At the same time, considering the vibration and noise generated by the interaction between the tire and the road surface, the main frequency range transmitted through the automobile structure is usually 20–300 Hz, and the body, suspension, and other structures usually resonate between 20–300 Hz. In addition, due to the influence of the acoustic-vibration coupling effect, the structural vibration is coupled to the acoustic cavity, and the process of eventually forming noise is affected by the modal characteristics of the vehicle body and the acoustic cavity resonance. The main frequency distribution of the interior noise matches the frequency distribution of the structural vibration, so the frequency band of the vibration acceleration is also 20–300 Hz.

Therefore, this paper mainly analyzes and discusses the 20–300 Hz frequency band of the collected data. The noise data shows the driver’s right ear noise data of a sample measured by the sound pressure sensor. Due to the large amount of vibration data collected in the test, the vibration acceleration data only shows the vibration acceleration of the left front shock absorber at the active end, the vibration acceleration of the front mounting point of the left front upper arm, the vibration acceleration of the rear mounting point of the left front upper arm, the vibration acceleration of the front subframe left front mounting point, and the vibration acceleration of the front subframe left rear mounting point, as shown in **Figure 8**.

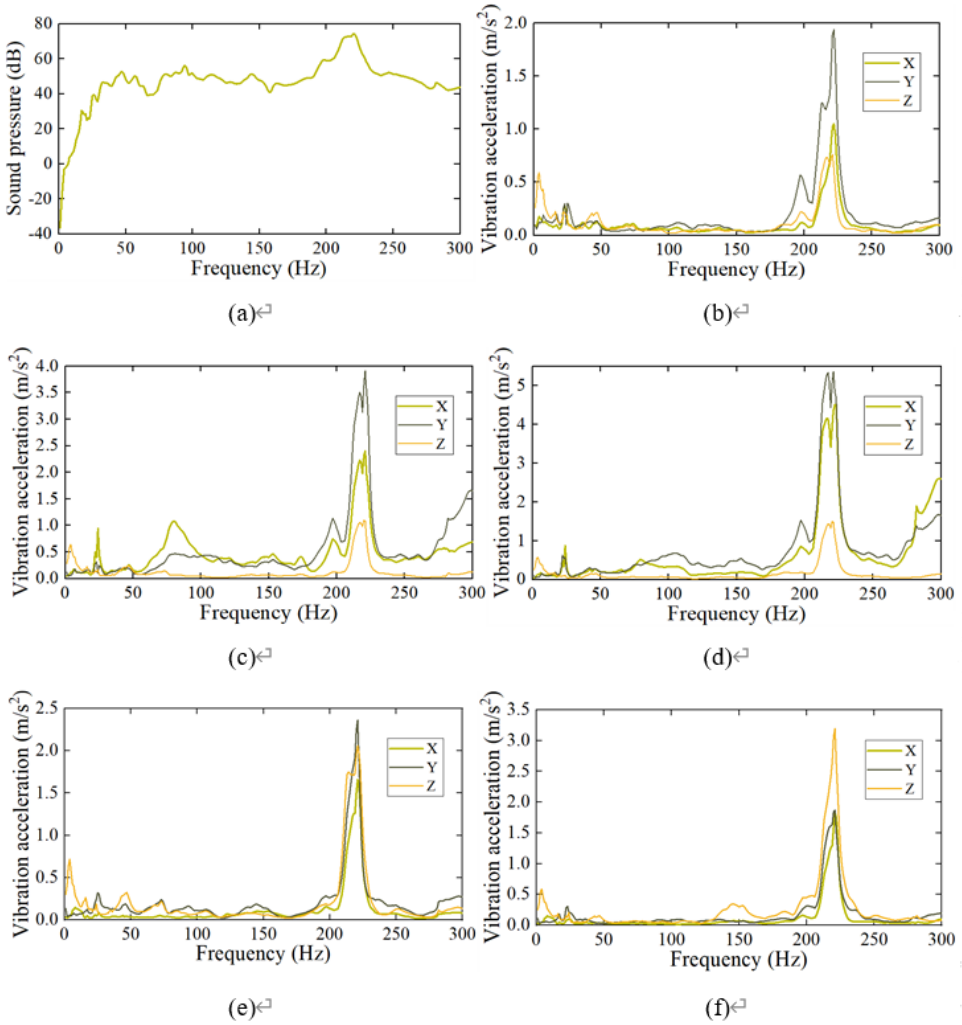

Figure 8. Test data: **(a)** Sample 1 driver's right ear noise; **(b)** left front shock absorber; **(c)** left front upper arm front mounting point; **(d)** left front upper arm rear mounting point; **(e)** front subframe left front mounting point; **(f)** front subframe left rear mounting point.

3.2. Simulation data collection

Based on the existing models of the enterprise, this study optimizes and adjusts the bushing, subframe, and body structure to improve the acoustic performance of the vehicle, especially the road noise control ability. In the research process, the mature vehicle simulation model is used to collect and analyze the road noise simulation data. In the modeling process, the simulation results of the vehicle model used in this study were verified by the key response parameters. In the long-term application, the accuracy of the model has also been verified by multiple rounds. The data results obtained by the model simulation are highly consistent with the real vehicle test data, which can accurately reflect the vibration and noise characteristics of the vehicle. Therefore, the simulation data can not only be used as an important research basis but also as a powerful supplement to the test data in order to reduce the test cost, improve the development efficiency, and provide strong support for further optimization of vehicle NVH performance. The data collection point in the simulation experiment is

consistent with the test process. In this paper, the NVH module of Hypermesh2021.1 is used to simulate the required data.

The noise response data is collected as the driver's right ear response. The acceleration data collection includes the vibration acceleration response of the active end and the acceleration response of the passive end. The transfer function collection mainly includes the IPI origin dynamic stiffness and the NTF noise transfer function. In the traditional CAE analysis process, engineers often need to carry out a large number of repetitive operations for the pre-processing and post-processing of the model. By setting the analysis condition in the form of the process tree of the Process Manager of NVH, the whole operation process of the frequency response function analysis can be fixed and simplified, which greatly reduces the workload of the pre-processing and post-processing of the simulation and avoids some errors caused by human negligence. The simulation setting of the transfer function first needs to enter the frequency response analysis module through the toolbar to set the frequency response definition process and complete the parameter setting of the entire analysis according to the process tree. In this paper, the global damping, SPC single-point constraint, and MPC multi-point constraint are set to zero. According to the above steps, the road noise response header file and the frequency response analysis header file are generated and imported into the required basic model, respectively. By systematically adjusting the key parameters of the model, such as bushing stiffness, elastic modulus, and structural thickness, the simulation data collection under different simulation models and different load conditions was obtained, and finally 100 sets of simulation sample data were collected. Due to the large amount of data, only two sets of examples of the effect of modifying the local bushing parameters on the driver's right ear noise response are shown, as shown in **Figure 9**.

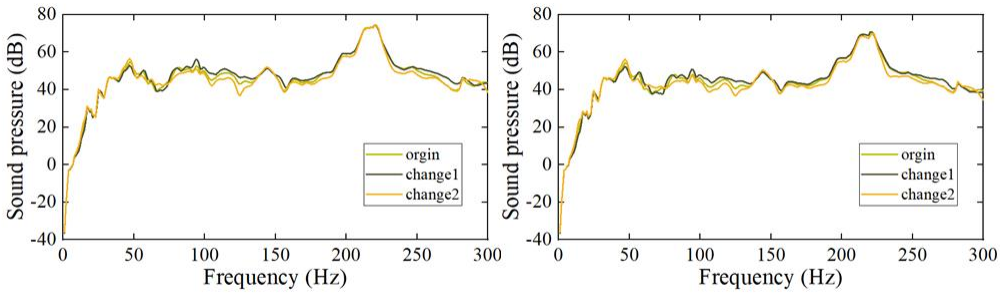

Figure 9. Test data: **(a)** Driver's right ear noise change1; **(b)** driver's right ear noise change2.

4. Road noise prediction model

4.1. Data preprocessing and model building

In order to eliminate the influence of data unit and magnitude difference, improve the stability and convergence speed of model training, and take into account the limitation of the model on the output data range, it is necessary to normalize the input data [44,45] and map it to the [0, 1] interval. The prediction model is calculated based

on the normalized data, and the final prediction result is restored to the original magnitude by anti-normalization. The normalized formula is shown in Equation (9):

$$y = (y_{\max} - y_{\min}) \times \frac{x - x_{\min}}{x_{\max} - x_{\min}} + y_{\min} \tag{9}$$

where x is the original data set, $x_{\max}$ is the maximum value of the data set, $x_{\min}$ is the minimum value of the data set, $y_{\max}$ is the upper limit of the normalized interval (take 1), and $y_{\min}$ is the lower limit of the normalized interval (take 0).

In the process of data import of the prediction model, reasonable division of data sets is the key to ensuring the training effect of the model and evaluating the generalization ability. Usually, the data set is divided into a training set, a test set, and a final verification set to ensure that the model can effectively learn data features and have good prediction ability. The training set is used for the training process of the model. By continuously adjusting the parameters, the model learns the rules between the data and optimizes the prediction effect. The test set is used to evaluate the performance of the model on unseen data, analyze its accuracy and stability, and determine whether there are over-fitting or under-fitting problems; the final validation set is used for the final evaluation after the model optimization is completed to ensure its reliability and generalization ability in practical applications. In this paper, 2 sets of test data and 100 sets of simulation data are integrated into a data set, and randomly disrupted. The data set is divided according to the ratio of 4:1. Among them, 80 sets of data are used for training, 20 sets of data are used for testing, and 2 sets of data are retained as the final verification set to ensure the adaptability of the model on different data and improve the confidence and practicability of the prediction results.

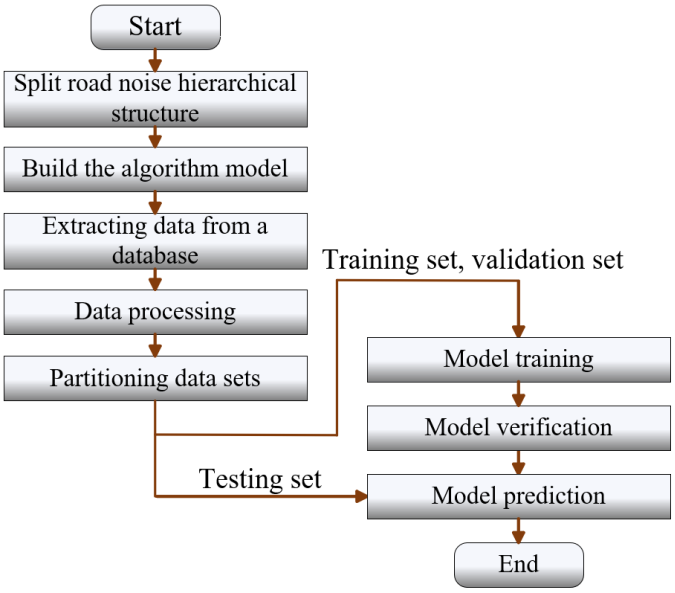

Figure 10. Prediction model building process.

GRU prediction model, LSTM prediction model, and CNN prediction model. Taking the driver's right ear noise prediction as an example, the input size of the GRU network and the LSTM network is 300 × 48, the output size is 300 × 1, the learning rate is set to 0.001, and the optimizer selects Adam; the input size of the CNN network is 300 × 48, the output size is 300 × 1, the number of channels is set to 12, the kernel

size is set to 2, the step size is set to 1, the learning rate is set to 0.001, the optimizer selects SGD, and the momentum is set to 0.9. By observing the change trend of the loss function and the prediction effect, the epoch of the three networks is set to 300, and the performance of the model is optimal or no longer significantly improved. As shown in **Figure 10**, the prediction model is built. After the data samples are imported and the data sets are divided according to the requirements, the network models are imported for training and testing. When the model training is completed and the model reaches a high accuracy, the verification set is imported to verify the generalization and accuracy of the prediction model.

4.2. Road noise model prediction and results comparison

The root mean square error (RMSE) can effectively measure the deviation between the predicted value and the true value of the model and is sensitive to large errors. The mean absolute error (MAE) provides a more intuitive mean error, which can effectively reflect the overall prediction error of the model. The coefficient of determination (R^2) measures the degree of fitting of the model to the target data and can show the model's ability to explain the data variation. These three indicators can comprehensively evaluate the accuracy and generalization ability of the prediction model. Therefore, RMSE, MAE, and R^2 are selected as evaluation indicators [46,47], and the calculation formulas of each indicator are as follows. On the other hand, the running time is an important index to measure the computational efficiency of the prediction model. In view of the fact that the road noise data processed in this study have the characteristics of large data scale and high computational cost, and in engineering applications, the model prediction efficiency directly affects its practical application value. Therefore, the model running time is included in the evaluation index system to comprehensively consider the performance of the model.

$$\mathrm{RMSE} = \sqrt{\frac{1}{n}\sum_{i=1}^{n}(y_i - \hat{y}_i)^2} \tag{10}$$

$$\mathrm{MAE} = \frac{1}{n}\sum_{i=1}^{n}|y_i - \hat{y}_i| \tag{11}$$

$$R^2 = 1 - \frac{\sum_{i=1}^{n}(\mathrm{y}_i - \hat{y}_i)^2}{\sum_{i=1}^{n}(y_i - \bar{y}_i)^2} \tag{12}$$

where n is the number of samples, y_i is the true value, $\hat{y}_i$ is the predicted value, $\bar{y}_i$ is the mean value of the true value.

In order to intuitively represent the prediction results of the road noise model, the prediction results of the GRU model, the LSTM model and the CNN model are compared with the real values, and the comparison diagram of the model prediction results shown in **Figure 11** is drawn. According to the analysis, the predicted value of the GRU model and the predicted value of the LSTM model, are in good agreement with the trend of the real value (label), which can reflect that the two models can

accurately predict the driver's right ear noise and realize the accurate prediction of road noise performance. In contrast, the predicted value of the CNN model is quite different from the true value, which is difficult to apply to the research object of this paper. This may be because noise prediction is a time-dependent task. Both the GRU model and the LSTM model are specifically used to capture and learn long-term dependencies in time series data, which can effectively capture time series patterns in signals. CNN is usually used to process local spatial features and has a weak ability to capture long-term trends in time series data. Therefore, based on the fact that the prediction task in this paper predicts the temporal variation of noise based on historical acceleration data, IPI data, NTF data, etc., LSTM and GRU are more suitable than CNN.

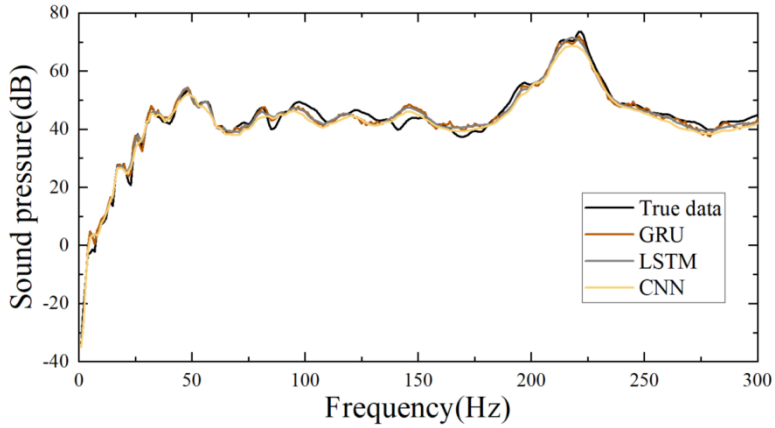

Figure 11. Comparison of model prediction results.

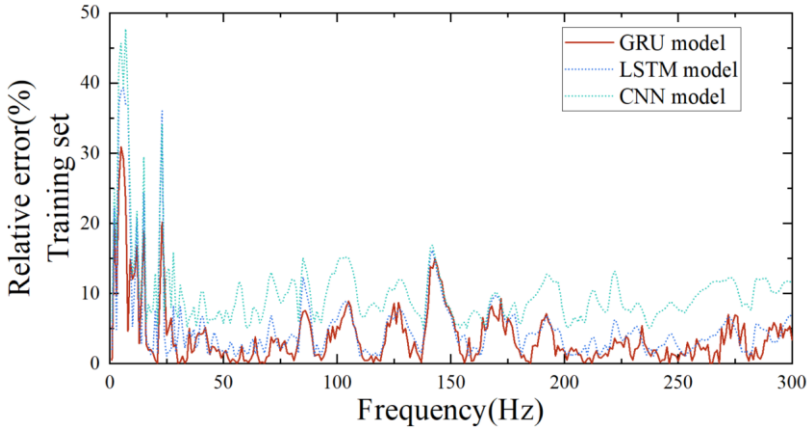

Figure 12. Comparison of model prediction errors.

In order to further compare the performance differences of GRU, LSTM, and CNN models in road noise prediction, this study analyzes the prediction errors of the three models in each frequency band in detail, as shown in **Figure 12**. The relative error curves of the three models at each frequency are shown in the figure. The results show that the relative errors of the three models have obvious abnormal peaks in the frequency range of 0–25 Hz. This phenomenon may be due to the poor response of the sound measurement equipment to the low-frequency band and the simplification of the low-frequency band by the simulation model. Due to the low amplitude of the noise signal itself and the significant noise interference, the low-frequency band of the

sample data obtained by the test and simulation is not accurate, which leads to the decrease of the prediction accuracy of the model. However, due to the limited influence of low-frequency signals below 25 Hz on the subjective noise perception of occupants, the error of this frequency band has little influence on the analysis of actual road noise problems. In addition, in the frequency band of more than 25 Hz, the relative error of the GRU model is lower than that of the LSTM and CNN models, which is close to the analysis results of **Figure 11**. This further verifies the advantages of the GRU model in dealing with temporal noise prediction tasks.

In order to quantitatively compare the specific advantages and disadvantages of the three models, the overall RMSE, MAE, R^2 and running time of the three models are recorded, as shown in **Table 1**. The RMSE value of the GRU prediction result is 2.18, the MAE value is 7.66%, and the R^2 value is 0.97. The RMSE value of the LSTM prediction result is 2.39, the MAE value is 8.03%, and the R^2 value is 0.96. The error results of the two models are small and better than the CNN model. The RMSE value is 5.26, the MAE value is 14.06%, and the R^2 value is 0.85. Although the accuracy difference between the prediction results of the GRU model and the LSTM model is small, the training time of the LSTM model is five times that of the GRU model, so the overall performance of the GRU model is the best.

Table 1. Statistical table of model error results and running time.

Index	CNN	LSTM	GRU
RMSE	5.26	2.39	2.18
MAE	14.06%	8.03%	7.66%
R^2	0.85	0.96	0.97
Time (s)	8.13	76.83	15.97

4.3. Verification of road noise model prediction results

The main role of the validation set is to evaluate the performance of the model on unknown data, help us select the best model and hyperparameters, and prevent overfitting [48–52]. It provides a basis for the optimization and tuning of the model and ensures that the model has good generalization ability in practical applications. In the model validation process, the validation set samples that are not involved in model training and model prediction are used to simulate new scenarios in practical applications so that the generalization ability of the model can be intuitively evaluated. In addition, by introducing a variety of models for verification and comparison, the generalization performance of the model is reflected by comparing and analyzing the prediction results of different models. The application of the validation set data in the prediction effect of the three models is shown in **Figure 13**. By observing the prediction results of sample 1 and sample 2 in the validation set, it can be seen that the conclusion is roughly the same as the analysis in Section 4.2. It is still the case that the predicted value of the GRU model and the predicted value of the LSTM model are better than the real value (label) trend, and the predicted value of the CNN model is quite different from the real value.

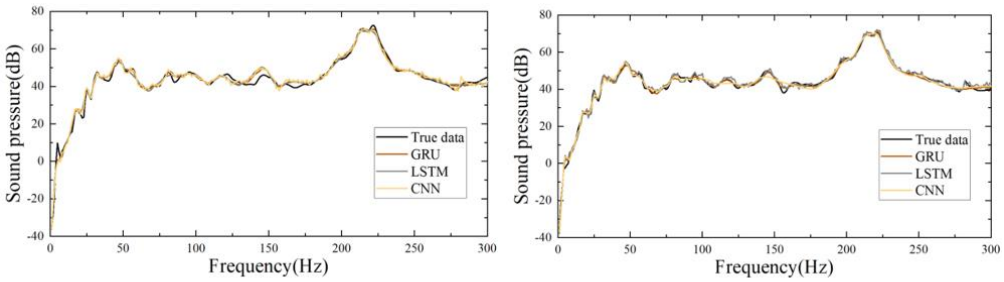

Figure 13. Verification set prediction results: **(a)** Comparison chart of prediction results of validation set sample 1; **(b)** comparison chart of prediction results of validation set sample 2.

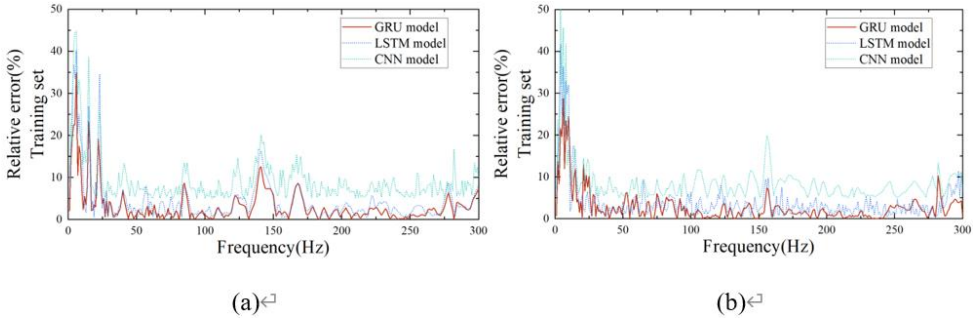

Figure 14. Validation set prediction error: **(a)** Comparison chart of prediction error of validation set sample 1; **(b)** comparison chart of prediction error of validation set sample 2.

Table 2. Verification set model error results and running time statistics table.

	Index	**CNN**	**LSTM**	**GRU**
Validation set sample 1	RMSE	5.5	2.39	2.47
	MAE	13.84%	8.30%	7.49%
	R^2	0.87	0.95	0.96
	Time (s)	9.04	69.88	15.04
Validation set sample 2	RMSE	4.81	1.73	1.73
	MAE	13.14%	7.12%	7.09%
	R^2	0.92	0.96	0.98
	Time (s)	12.08	70.89	15.15

In order to further quantify and compare the prediction performance differences of GRU, LSTM, and CNN models on the validation set, this study conducted a statistical analysis of the prediction errors of the three models. The specific results are shown in **Figure 14** and **Table 2**. The results show that the prediction effects of the CNN model, LSTM model, and GRU model are relatively stable. The RMSE value of the CNN model on sample 1 is 5.50, the MAE value is 13.84%, and the R^2 value is 0.87. The RMSE value on sample 2 is 4.81, the MAE value is 13.14%, and the R^2 value is 0.92. The RMSE value of the LSTM model on sample 1 is 2.39, the MAE value is 8.30%, and the R^2 value is 0.95. The RMSE value on sample 2 is 1.73, the MAE value is 7.12%, and the R^2 value is 0.96. The RMSE value of the GRU model

on sample 1 is 2.47, the MAE value is 7.49%, and the R^2 value is 0.96. The RMSE value on sample 2 is 1.73, the MAE value is 7.09%, and the R^2 value is 0.98. The accuracy and reliability of the GRU model and LSTM model are still better than the CNN model. In addition, the running time of the validation set samples on the two models was observed. The LSTM model was 69.88 and 70.89, and the GRU model was 15.04 and 15.15. The running time of the GRU model is a quarter to a fifth of the running time of the LSTM model, and its efficiency is significantly better than the LSTM model.

In addition, the prediction performance of the proposed model on the verification set can also reflect its adaptability and generalization. On this basis, a small amount of relevant data from other models can be supplemented, and the model can be fine-tuned to realize the effective migration and application of the model on different models or roads. With the continuous accumulation of the number of samples, the prediction performance of the model will continue to improve iteratively.

5. Conclusion

Based on the analysis of the road noise generation mechanism and transfer path, this paper constructs a hierarchical structure of vehicle road noise with the body system as the core and emphasizes the excitation, transfer function, and response of the vehicle body to right ear noise. On the basis of avoiding the complex structure of suspension and frame, the noise transfer function (NTF) and the origin dynamic stiffness (IPI) are introduced as the research parameters, and multiple critical paths of road noise are re-divided to realize the fusion modeling of transfer function, vibration acceleration, and bushing dynamic stiffness. Aiming at the problem of insufficient samples, 100 groups of representative data samples are generated in batches through parametric design and CAE simulation, and a data sample library with self-consistent fusion of mechanism and data is constructed. Finally, the TPA analysis and data-driven method are combined, and the empirical formula is introduced as the loss term to establish a road noise performance prediction model based on self-consistent fusion of mechanism and data. The results show that the model has excellent performance in prediction accuracy, robustness, and operation efficiency. Among them, the GRU model performs best (RMSE = 2.18, MSE = 7.66%, time = 15.97 s), which is significantly better than the comparison method.

Author contributions: Conceptualization, YM and RD; methodology, TL and RD; software, RD; validation, HH, QY and MW; investigation, HH; writing—original draft preparation, YM and RD; writing—review and editing, RD; visualization, QY; supervision, MW; funding acquisition, TL. All authors have read and agreed to the published version of the manuscript.

Funding: This research was funded by China FAW Corporation Limited, grant number RBJ37-ZX.

Acknowledgments: The authors would like to acknowledge the support from the Institute of Energy and Power Research for the experimental research.

Availability of data and materials: The authors do not have permission to share the data.

Conflict of interest: The authors declare no conflict of interest.

References

1. Xue H, Previati G, Gobbi M, et al. Research and Development on Noise, Vibration, and Harshness of Road Vehicles Using Driving Simulators—A Review. SAE International Journal of Vehicle Dynamics, Stability, and NVH. 2023; 7(4). doi: 10.4271/10-07-04-0035
2. Huang H, Huang X, Ding W, et al. Vehicle vibro-acoustical comfort optimization using a multi-objective interval analysis method. Expert Systems with Applications. 2023; 213: 119001. doi: 10.1016/j.eswa.2022.119001
3. Huang H, Lim TC, Wu J, et al. Multitarget prediction and optimization of pure electric vehicle tire/road airborne noise sound quality based on a knowledge- and data-driven method. Mechanical Systems and Signal Processing. 2023; 197: 110361. doi: 10.1016/j.ymssp.2023.110361
4. Diez-Ibarbia A, Battarra M, Palenzuela J, et al. Comparison between transfer path analysis methods on an electric vehicle. Applied Acoustics. 2017; 118: 83-101. doi: 10.1016/j.apacoust.2016.11.015
5. Cervantes-Madrid G, Peral-Orts R, Campillo-Davo N, et al. Inverse transfer path analysis, a different approach to shorten time in NVH assessments. Applied Acoustics. 2021; 181: 108178. doi: 10.1016/j.apacoust.2021.108178
6. Zhu P, Wang Z, Qin Z, et al. The transfer path analysis method on the use of artificial excitation: Numerical and experimental studies. Applied Acoustics. 2018; 136: 102-112. doi: 10.1016/j.apacoust.2018.02.007
7. Li M, Zhu Z, Deng T, et al. An investigation into high-speed train interior noise with operational transfer path analysis method. Railway Engineering Science. 2021; 29(1): 1-14. doi: 10.1007/s40534-021-00235-0
8. Vaitkus D, Tcherniak D, Brunskog J. Application of vibro-acoustic operational transfer path analysis. Applied Acoustics. 2019; 154: 201-212. doi: 10.1016/j.apacoust.2019.04.033
9. Liu W, Huang H, Fan D, et al. An LSTM-based method for predicting road noise in automobiles. Noise and vibration control. 2023; 3: 145-152. doi: 10.3969/j.jssn.1006-1355.2023.03.023
10. Rapino L, Ripamonti F, Dallasta S, et al. Synthesis of equivalent sources for tyre/road noise simulation and analysis of the vehicle influence on sound propagation. Applied Acoustics. 2024; 216: 109751. doi: 10.1016/j.apacoust.2023.109751
11. Bartolozzi G, Danti M, Camia A, et al. Enhancement of Full-Vehicle Road Noise Simulation Including Detailed Road Surface and Innovative Tire Modeling. SAE International Journal of Passenger Cars - Mechanical Systems. 2016; 9(3): 1091-1099. doi: 10.4271/2016-01-1827
12. Su J, Lou J, Jiang X. Research on optimization control of vehicle road noise performance. IOP Conference Series: Earth and Environmental Science. 2021; 769(4): 042055. doi: 10.1088/1755-1315/769/4/042055
13. Yoshida J, Tanaka K, Nakamoto R, et al. Combination Analysis of Operational TPA and CAE Technique for Obtaining High Contributing Vibration Mode. SAE Technical Paper Series; 2017. doi: 10.4271/2017-01-1856
14. Harbi Y, Medani K, Gherbi C, et al. Roadmap of Adversarial Machine Learning in Internet of Things-Enabled Security Systems. Sensors. 2024; 24(16): 5150. doi: 10.3390/s24165150
15. Huang HB, Wu JH, Huang XR, et al. The development of a deep neural network and its application to evaluating the interior sound quality of pure electric vehicles. Mechanical Systems and Signal Processing. 2019; 120: 98-116. doi: 10.1016/j.ymssp.2018.09.035
16. Wang J, Han H, Han X, et al. Reinforcement learning path planning method incorporating multi-step Hindsight Experience Replay for lightweight robots. Displays. 2024; 84: 102796. doi: 10.1016/j.displa.2024.102796
17. Zhao J, Yin Y, Chen J, et al. Evaluation and Prediction of Vibration Comfort in Engineering Machinery Cabs Using Random Forest with Genetic Algorithm. SAE International Journal of Vehicle Dynamics, Stability, and NVH. 2024; 8(4). doi: 10.4271/10-08-04-0027
18. An LS, Jung S. Data-driven prediction of wind pressure on low-rise buildings in complex heterogeneous terrains. Building and Environment. 2024; 265: 112022. doi: 10.1016/j.buildenv.2024.112022
19. Chen L, Zhang K, Yan J. Data-driven study on shear bearing capacity of segmental concrete joints. Structures. 2024; 68: 107145. doi: 10.1016/j.istruc.2024.107145
20. Oh JY, Jung HW, Lee MH, et al. Enhancing active noise control of road noise using deep neural network to update secondary path estimate in real time. Mechanical Systems and Signal Processing. 2024; 206: 110940. doi: 10.1016/j.ymssp.2023.110940

21. Luo YK, Chen SX, Zhou L, et al. Evaluating railway noise sources using distributed microphone array and graph neural networks. Transportation Research Part D: Transport and Environment. 2022; 107: 103315. doi: 10.1016/j.trd.2022.103315
22. Sun P, Dai R, Li H, et al. Multi-Objective Prediction of the Sound Insulation Performance of a Vehicle Body System Using Multiple Kernel Learning–Support Vector Regression. Electronics. 2024; 13(3): 538. doi: 10.3390/electronics13030538
23. Huang H, Wang Y, Wu J, et al. Prediction and optimization of pure electric vehicle tire/road structure-borne noise based on knowledge graph and multi-task ResNet. Expert Systems with Applications. 2024; 255: 124536. doi: 10.1016/j.eswa.2024.124536
24. Guo R, Wang J, Yuan Y, et al. Interpretation of dual time-dependent chloride diffusion in concrete based on physical information neural networks. Case Studies in Construction Materials. 2024; 21: e03769. doi: 10.1016/j.cscm.2024.e03769
25. Cong J, Liu Z, Zhou S, et al. Predicting fatigue life and crack growth rate of TC4 titanium alloy based on PINN before and after ultrasonic impact treatment. Engineering Failure Analysis. 2024; 166: 108875. doi: 10.1016/j.engfailanal.2024.108875
26. Liu CX, Wang X, Liu W, et al. A physics-informed neural network for Kresling origami structures. International Journal of Mechanical Sciences. 2024; 269: 109080. doi: 10.1016/j.ijmecsci.2024.109080
27. Fan JL, Zhu G, Zhu ML, et al. A data-physics integrated approach to life prediction in very high cycle fatigue regime. International Journal of Fatigue. 2023; 176: 107917. doi: 10.1016/j.ijfatigue.2023.107917
28. Jeong H, Bai J, Batuwatta-Gamage CP, et al. A Physics-Informed Neural Network-based Topology Optimization (PINNTO) framework for structural optimization. Engineering Structures. 2023; 278: 115484. doi: 10.1016/j.engstruct.2022.115484
29. Pang J, Mao T, Jia W, et al. Prediction and Analysis of Vehicle Interior Road Noise Based on Mechanism and Data Series Modeling. Sound & Vibration. 2024; 58(1): 59-80. doi: 10.32604/sv.2024.046247
30. Fan D, Dai P, Yang M, et al. Research on Maglev Vibration Isolation Technology for Vehicle Road Noise Control. SAE International Journal of Vehicle Dynamics, Stability, and NVH. 2022; 6(3). doi: 10.4271/10-06-03-0016
31. Del Pizzo LG, Bianco F, Moro A, et al. Relationship between tyre cavity noise and road surface characteristics on low-noise pavements. Transportation Research Part D: Transport and Environment. 2021; 98: 102971. doi: 10.1016/j.trd.2021.102971
32. Yang M, Dai P, Yin Y, et al. Predicting and optimizing pure electric vehicle road noise via a locality-sensitive hashing transformer and interval analysis. ISA Transactions. 2025; 157: 556-572. doi: 10.1016/j.isatra.2024.11.059
33. Cao Y, Hou H, Liu Y, et al. Sound Pressure Level Control Methods for Electric Vehicle Active Sound Design. SAE International Journal of Vehicle Dynamics, Stability, and NVH. 2021; 5(2). doi: 10.4271/10-05-02-0014
34. Li Q, Ripamonti F, Corradi R, et al. Simulation of deterministic tyre noise based on a monopole substitution model. Applied Acoustics. 2021; 178: 108009. doi: 10.1016/j.apacoust.2021.108009
35. Duan Y, Wu J, Zhang Y. Kinematics characteristics of unsprung mass in a double wishbone suspension based on velocity transformation. Acta Mechanica Sinica. 2024; 41(2). doi: 10.1007/s10409-024-23661-x
36. Zhang S, Gao Y, Gao D, et al. Serial combinational optimization method for double wishbone suspension's pseudo damage improvement. Structural and Multidisciplinary Optimization. 2023; 66(6). doi: 10.1007/s00158-023-03579-9
37. Schmitz T. Chassis concept of the individually steerable five-link suspension: a novel approach to maximize the road wheel angle to improve vehicle agility. Automotive and Engine Technology. 2024; 9(1). doi: 10.1007/s41104-024-00142-6
38. Alizadeh R, Fataliyev V, Akhundov E. Improving the Design of the Linkage Suspension of a Robotic Mobile Modular System. Journal of Machinery Manufacture and Reliability. 2024; 53(6): 539-543. doi: 10.1134/s1052618824701322
39. Xu M, Han Y, Zhu N, et al. A method for recognizing individual dynamic thermal adaptations using wireless signals. Energy and Buildings. 2025; 333: 115448. doi: 10.1016/j.enbuild.2025.115448
40. Choi SW, Li Y, Yang X, et al. Reachability analysis of recurrent neural networks. Nonlinear Analysis: Hybrid Systems. 2025; 56: 101581. doi: 10.1016/j.nahs.2025.101581
41. Zeng C, Xu C, Li H, et al. A novel ensemble learning model for state of health estimation of lithium-ion batteries. Journal of Power Sources. 2025; 638: 236608. doi: 10.1016/j.jpowsour.2025.236608
42. Huang H, Huang X, Ding W, et al. Optimization of electric vehicle sound package based on LSTM with an adaptive learning rate forest and multiple-level multiple-object method. Mechanical Systems and Signal Processing. 2023; 187: 109932. doi: 10.1016/j.ymssp.2022.109932
43. National Acoustics Standardization Technical Committee. Acoustics-Measurement Method for In-vehicle Noise of Automobiles: GB/T 18697-2002. Beijing: China Standard Press; 2002.
44. Xu S, Dai Y, Yan C, et al. On the preprocessing of physics-informed neural networks: How to better utilize data in fluid mechanics. Journal of Computational Physics. 2025; 528: 113837. doi: 10.1016/j.jcp.2025.113837

45. Sagar N, Suresh KP, Sridhara S, et al. Precision detection of grapevine downy and powdery mildew diseased leaves and fruits using enhanced ResNet50 with batch normalization. Computers and Electronics in Agriculture. 2025; 232: 110144. doi: 10.1016/j.compag.2025.110144
46. Yang Y, Zhao Q, Yang J. Optimization-Based Parameter Identification for Coupled Biodynamic Model of Seated Posture under Vibration. SAE International Journal of Vehicle Dynamics, Stability, and NVH. 2022; 6(2). doi: 10.4271/10-06-02-0011
47. Trivedi R, Singh TN, Raina AK. Simultaneous prediction of blast-induced flyrock and fragmentation in opencast limestone mines using back propagation neural network. International Journal of Mining and Mineral Engineering. 2016; 7(3): 237. doi: 10.1504/ijmme.2016.078350
48. Sathe S, Samak C, Samak T, et al. Data Driven Vehicle Dynamics System Identification Using Gaussian Processes. SAE Technical Paper Series; 2024. doi: 10.4271/2024-01-2022
49. Liu Y, Cai K, Tian Z. A 3D discrete modeling strategy for predicting the cooling performance of the central cone laminate. Applied Thermal Engineering. 2025; 269: 125998. doi: 10.1016/j.applthermaleng.2025.125998
50. Petrone B, Giovannardi E, Brusa A, et al. Development of an Automatic Pipeline for Data Analysis and Pre-Processing for Data Driven-Based Engine Emission Modeling in a Real Industrial Application. SAE Technical Paper Series; 2024. doi: 10.4271/2024-01-2018
51. Wu Y, Li T, Zhang R, et al. Establishment of nomogram of early death in elderly pancreatic cancer patients with liver metastasis. Discover Oncology. 2025; 16(1). doi: 10.1007/s12672-025-02059-4
52. Huang H, Huang X, Ding W, et al. Uncertainty optimization of pure electric vehicle interior tire/road noise comfort based on data-driven. Mechanical Systems and Signal Processing. 2022; 165: 108300. doi: 10.1016/j.ymssp.2021.108300